Shape-Selective Formation of Monodisperse Copper Nanospheres and Nanocubes *via* Disproportionation Reaction Route and Their Optical Properties

Huizhang Guo,[†] Yuanzhi Chen,*[,†] Michael B. Cortie,[‡] Xiang Liu,[†] Qingshui Xie,[†] Xiang Wang,[§] Dong-Liang Peng*[,†]

† Department of Materials Science and Engineering, College of Materials, Xiamen University, Xiamen 361005, China.

‡ Institute for Nanoscale Technology, University of Technology, Sydney, PO Box 123, Broadway, NSW 2007, Australia.

§ College of Chemistry and Chemical Engineering, Xiamen University, Xiamen 361005, China.

ABSTRACT: Synthesis of stable and monodisperse Cu nanocrystals of controlled morphology has been a long-standing challenge. In this article, we report a facile disproportionation reaction approach for the synthesis of such nanocrystals in organic solvents. Either spherical or cubic shapes can be produced, depending on conditions. The typical Cu nanospheres are single crystals with a size of 23.4±1.5 nm, and can self-assemble into three-dimensional (3D) nanocrystal superlattices with a large scale. By manipulating the chemical additives, monodisperse Cu nanocubes with tailorable sizes have also been obtained. The probable formation mechanism of these Cu nanocrystals is discussed. The narrow size distribution results in strong surface plasmon resonance (SPR) peaks even though the resonance is located in the interband transition region. Double SPR peaks are observed in the extinction spectra for the Cu nanocubes with relative large sizes. Theoretical simulation of the extinction spectra indicates that the SPR band located at longer wavelengths is caused by assembly of Cu nanocubes into more complex structures. The synthesis procedure that we report here is expected to foster systematic investigations on the physical properties and self-assembly of Cu nanocrystals with shape and size singularity for their potential applications in photonic and nanoelectronic devices.

KEYWORDS: crystal growth, synthetic methods, self-assembly, nanocrystals, optics

INTRODUCTION

Group IB metallic nanostructures, such as Cu, Ag and Au nanocrystals, are of particular interest as an important class of photonic components because of the interactions between their free electrons and light. This interaction results in surface plasmon resonances (SPR) at specific wavelengths. The unique optical properties of these nanocrystals, including the SPR effect and its associated light scattering, have enabled them to be widely used. Applications include enhancing light trapping and absorption for improving the performance of solar cells,[1,2] providing substrates for the surface-enhanced Raman spectroscopy of trace chemical species,[3,4] and providing ultrasensitive refractometric biosensors.[5]

It is well known that the shape and size play important roles in determining the number, position and intensity of SPR modes.[6-9] Moreover, a narrow size distribution is vital to induce a strong SPR signal at a specific wavelength. In the past decade, appreciable achievements have been made in the shape-controlled synthesis of noble metal nanocrystals, such as Au and Ag, with various morphologies.[7,10,11] However, comparable success with Cu has been elusive.[12] Reasons for this include the relatively poorer oxidation resistance of Cu nanostructures and the lack of shape control.

Nevertheless, given that Cu has a relatively low cost compared to noble metals, it may be useful to develop a facile strategy to prepare Cu nanocrystals with controllable shape and size distribution, as well as a better understanding of the role of shape in their optical responses. About one decade ago, Pileni and co-workers had concentrated their efforts on understanding the growth mechanism of Cu nanocrystals of differing shapes[13] as well as tuning their optical properties.[14] Zhong et al. also tried to control the shape and size of Cu nanocrystals in organic

solvents with molecular capping agents and reaction temperature.[15] Pastoriza-Santos *et al.* synthesized single-crystalline Cu nanoplates through reduction of copper salts by hydrazine with polyvinyl pyrrolidone as a stabilizer. An intense in-plane SPR band was observed in these Cu nanoplates.[16] Recently, Xia et al. were able to synthesize Cu nanocrystals with controllable shapes.[17] Progress has also been made in fabrication of Cu nanowires,[18-20] nanocubes[17,20] and nanospheres.[21,22] Nevertheless, preparation of Cu nanocrystals with monodisperse size distribution is still a difficult task. The conflict stems partially from the fact that strong reducing agents or high temperatures are normally required to reduce cupric ions into zero valent atoms because of the relatively low reduction potential of Cu^{2+}. However, under such drastic reaction conditions, control of the shape of nanocrystals may be lost due to aggregative growth and Ostwald ripening.[23,24] Another challenge is the propensity of Cu nanocrystals to oxidize. As a consequence, in order to synthesize monodisperse Cu nanocrystals in solution, it is necessary to pay attention to the way by which zero valent Cu atoms are generated. This may be done by modulating the redox potentials of the metal ions as well as by controlling the growth and ripening rate with stabilizing agents.

Previous research normally supposed that surfactants only served as capping agents or adsorbates[25-27] which played important roles in shape-selective synthesis of anisotropic nanocrystals as well as in controlling particle size distribution. However, the possible multiple roles of the surfactant molecules and anions in solvents should not be ignored. For instance, modification of the redox potential of the metal (owing to the coordination effect between metallic ions and surfactant molecules or anions) may have a considerable influence on the synthesized nanocrystals.[27,28] For example, Sun and Peng demonstrated how such complexation could be used to generate single-crystalline Ag nanocubes in a mixed solvent of octyl ether and

oleylamine in the presence of Cl^- ions (from dimethyldistearylammonium chloride) at 260 ^oC.[29] It should be noted that the shape and size of Ag nanocrystals would be difficult to control in the absence of Cl^- ions at such a high temperature. Recently, Tuan and coworkers reported the synthesis of Cu nanocubes with an average edge length of 75.7 nm using an injection approach that involved the fast reduction of CuCl.[30] A similar result was also demonstrated in our recent research on the shape-controlled synthesis of CuNi alloyed nanoplates[31] and Cu nanowires.[20] The strong coordination effect between Cu^{2+} and Cl^- ions prevented Cu^{2+} ions from being reduced by oleylamine. Therefore, Ni^{2+} ions were introduced into the reaction to act as catalysts to promote the reduction of Cu^{2+}, which enabled a controlled reduction rate of Cu^{2+} ions through controlling the reduction rate of Ni^{2+} ions by selective addition of surfactant molecules. This phenomenon provides a possible route to tune the nucleation rates of metal nanocrystals by modifying the coordination agents and surface adsorbates in solvents so as to keep the formation of Cu nanocrystals under kinetic control.

In the present work we exploit these insights to demonstrate a facile disproportionation reaction route in organic solvents for the synthesis of Cu nanocrystals with a tight size distribution. In our syntheses, no Ni^{2+} species are required to be added to promote the reduction of Cu^{2+}. In addition, CuBr is employed as Cu precursor and the reaction temperature (210-260 ^oC) is much lower than that (330 ^oC) reported in a previous study.[30] To the best of our knowledge this is the first time that monodisperse Cu nanocrystals with both spherical and cubic morphologies have been achieved *via* such a simple one-pot disproportionation reaction. The growth mechanism of as-prepared Cu nanocrystals has also been elucidated. We will show that bromide anions along with other capping agents are indispensable for the shape-selective formation of Cu nanocrystals with such a narrow size distribution. Finally, theoretical

simulations of the extinction spectra of the as-prepared Cu nanocrystals were undertaken to better understand their optical properties.

EXPERIMENTAL SECTION

Chemicals. Oleylamine (80~90%) and tri-octylphosphine oxide (TOPO, 90%) were purchased from Acros Organics. Tri-octylphosphine (TOP, 90%) was purchased from Sigma-Aldrich. Toluene, n-hexane, acetone, ethanol and CuBr were purchased from Sinopharm Chemical Reagent Co., Ltd. All of these chemicals were used as received without any further purification. It should be noted that it is very important to keep TOP from being oxidized in order to prepare monodispersed Cu nanospheres.

Synthesis of Monodisperse Cu Nanospheres. All of the syntheses were carried out with a protective atmosphere of argon. Typically, oleylamine (7 mL) and CuBr (0.6 mmol) were mixed in a three-necked flask by strong magnetic stirring at 80 ^{o}C for 15 min, then TOP (1 mmol) was injected into the obtained green solution, which immediately became colorless. After an additional stirring at 80 ^{o}C for 5 min, the mixed solution was heated up to 260 ^{o}C quickly and kept at this temperature for 3 h before cooling down to room temperature naturally. Excess hexane was added to the bright reddish solution, and the Cu nanospheres were precipitated out by centrifugation. The Cu nanospheres were purified by three rounds of centrifugation/redispersion in a mixed solution of hexane and acetone prior to being finally dispersed into toluene by ultrasonication for 30 min.

Self-Assembly of Monodisperse Cu Nanospheres into 3D Superlattices. A silicon wafer (5 mm×5 mm) which had been rinsed with hydrofluoric acid solution (5%) and acetone continuously was placed on the bottom of a penicillin bottle (5 mL). Toluene solution (2 mL)

containing Cu nanospheres was added into the penicillin bottle. After that, the penicillin bottle was kept in a thermostat until all of the toluene solution had evaporated.

Synthesis of Monodisperse Cu Nanocubes. All of the syntheses were carried out with a protective atmosphere of argon. Typically, CuBr (0.6 mmol) and TOPO (1.5 mmol) were dissolved into oleylamine (7 mL) in a three-necked flask by strong magnetic stirring at 80 ^{o}C for 15 min. Then the resulting solution was heated up to 260 ^{o}C quickly and refluxed at this temperature for 1 h before cooling down to room temperature naturally. The remaining steps are the same as those for preparing Cu nanospheres.

In order to obtain Cu nanocubes with a larger edge length (e.g. 76.4 nm), the content of TOPO was reduced to 0.5 mmol, while the aging time was increased to 2.5 h. In contrast, Cu nanocubes with an average edge length of about 31.5 nm were synthesized by decreasing the reaction temperature to 220 ^{o}C and aging at this temperature for 1 h. For the synthesis of Cu nanocubes with an average edge length of 24.1 nm, CuBr (0.6 mmol) and TOPO (5 mmol) were dissolved into 2 ml of oleylamine in a three-necked flask by strong magnetic stirring at 80 ^{o}C for 15 min. Then, the resulting solution was heated up to 210 ^{o}C quickly and refluxed at this temperature for 1 h before cooling down to room temperature naturally. Similarly, monodisperse Cu nanocubes with an average edge length of about 26.8 nm were achieved by prolonging the reaction time to 3 h.

Characterization. The samples for transmission electron microscopy (TEM) analyses were prepared by dropping the particle suspensions in toluene onto a Mo grid coated with carbon film before drying at room temperature under ambient conditions. TEM images and selective area electron diffraction (SAED) patterns were collected on a JEOL JEM-2100 transmission electron

microscope operating at 200 kV, while high-resolution TEM (HRTEM) images were collected on a FEI TECNAI F30 transmission electron microscope operating at 300 kV. The scanning electron microscopy (SEM) images were collected on a LEO 1530 scanning electron microscope operating at 15 kV. X-ray diffraction (XRD) measurements were taken on a Panalytical X'pert PRO diffractometer using Cu K_α radiation, operating at 40 kV and 30 mA. Visible-near infrared (NIR) extinction spectra were obtained at room temperature with a Shimadzu UV-2550 ultraviolet-visible spectrophotometer. Auger spectra were acquired with a PHI-610 scanning Auger microprobe. Fourier transform infrared (FTIR) spectra were obtained with a Thermo Fisher Scientific IS10 FTIR spectrometer.

Simulations. The optical extinction properties of single Cu nanocubes and their aggregates were simulated using the discrete dipole approximation (DDA) as implemented in the DDSCAT code of Draine and Flatau.[32] Version 7.1 of the code was used. In this scheme the shape is represented by an array of polarizable dipoles and the interaction with an incident periodic wave solved numerically. Metallic targets, in which the complex refractive index can have a large magnitude, require very long computation times and closely spaced dipoles in order to obtain converged results. The dielectric data for Cu and toluene were obtained from the literature.[33-35]

RESULTS AND DISCUSSION

Monodisperse Cu Nanospheres. Monodisperse Cu nanospheres have been synthesized using TOP as a chemical additive. Figure 1a shows the TEM image of the two-dimensional stacking pattern of 2-3 layers of the as-synthesized Cu nanospheres assembling on the amorphous carbon film. The size distribution histogram from the TEM image (Figure S1 and S2) reveals that the spheres have a relatively tight distribution of diameters with an average diameter of 23.4±1.5 nm.

Figure 1b displays the XRD pattern of the products prepared in the typical procedure. The diffraction peaks located at 43.3°, 50.4°, 74.1° and 90.1° can be assigned to the {111}, {200}, {220} and {311} planes of face-centered-cubic (fcc) Cu (JCPDS #03-1018). No diffraction peaks belonging to Cu_2O are observed, revealing the pure-phase nature and excellent oxidation resistance of the products, which may be attributed to the protection of surface adsorbed Br^- ions and surfactants. HRTEM images from a single Cu nanosphere observed along the [011] and [001] zone axes along with the fast Fourier transform (FFT) patterns are shown in Figure 1c and 1d, respectively. Well-aligned lattices without any twin structures indicate that the Cu nanosphere is a single crystal covered by a mixture of {011}, {111} and {100} facets on the surface (also see Figure S3). It should be note that it is not easy to tailor the size of monodisperse Cu nanospheres using the recipe described in the experimental section. In order to obtain Cu nanospheres with a smaller diameter, CuBr was replaced by copper acetylacetonate as a precursor, while TOPO was used to replace TOP (please find the synthetic details in Supporting Information). As a result, monodisperse Cu nanospheres with an average diameter of 12.6 nm were obtained (Figure 1e and S4).

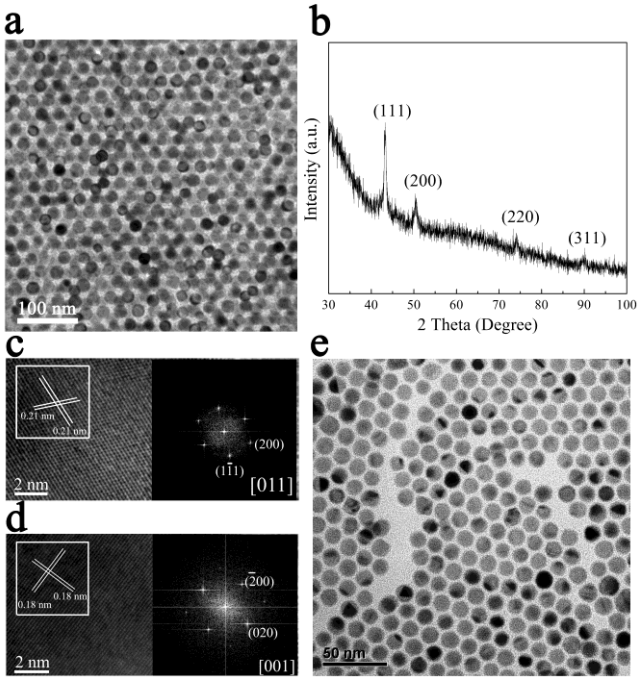

Figure 1. (a) and (b) are the TEM image and XRD pattern of the monodisperse Cu nanospheres with an average diameter of 23.4 nm, respectively. (c) and (d) are the HRTEM images of a single Cu nanosphere viewed along [011] and [001] zone axes, respectively. The right images in (c) and (d) are corresponding FFT patterns acquired from the square marking areas. (e) TEM image of monodisperse Cu nanospheres with an average diameter of 12.6 nm.

Owing to their very narrow size distribution and excellent dispersity in toluene solution, three-dimensional (3D) superlattices of multi-layer Cu nanospheres deposited on silicon wafer are acquirable during a slow evaporation of toluene in a thermostat. The self-assembly procedure is schematically illustrated in Figure S5. As can be seen from Figure S6, a lustrous liquid film on the surface of Cu nanosphere colloid forms and it becomes brighter and brighter as the evaporation of toluene proceeds. This is due to the assembling of Cu nanospheres on the air/liquid interface, which will finally land on the silicon substrate. Figure 2a to 2d display the SEM images of 3D superlattice formed by the monodisperse Cu nanospheres with an average

diameter of 23.4 nm with different magnifications, demonstrating that the as-synthesized monodispersed Cu nanospheres can self-assemble into a millimeter scaled 3D superlattices. The thickness of the 3D superlattice of Cu nanospheres is estimated to be more than twenty layers through the observation on the broken edges or "cracks" which result from the surface tension stress created during the evaporation of solvent.

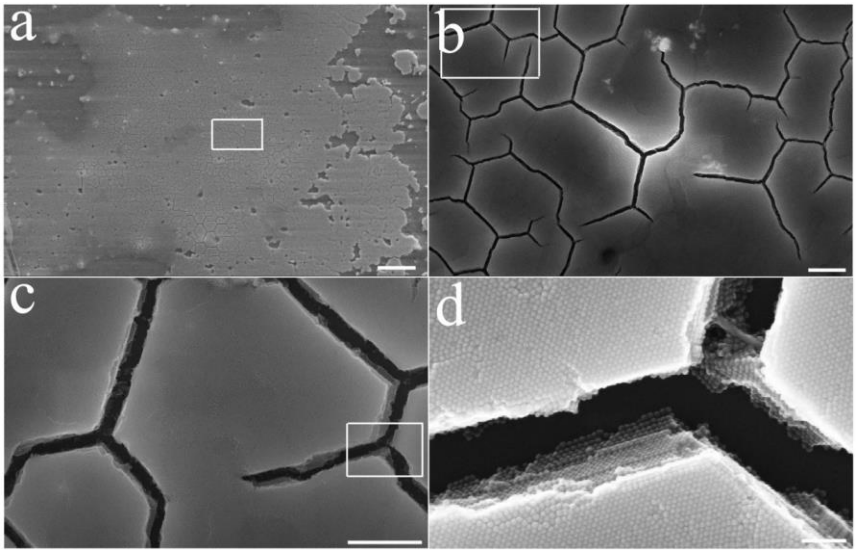

Figure 2. SEM images of the 3D superlattices composed of 23.4 nm Cu nanospheres with different magnifications. Images b, c and d are taken from the square frame shown in the previous one. The bar scales in a, b, c and d are 20 μm, 1 μm, 1 μm and 200 nm, respectively.

Monodisperse Cu Nanocubes. Monodisperse Cu nanocubes can be obtained if TOP is replaced by TOPO and the reaction time is shortened to one hour in the typical procedure for the synthesis of monodisperse Cu nanospheres. A representative TEM image of the as-synthesized Cu nanocubes is presented in Figure 3a, where only cubes are observed, indicating a good uniformity of shape. The Cu nanocubes have a narrow size distribution with an average edge length of 46.8 nm (see size distribution histogram in Figure S7). Figure 3b shows the XRD

pattern of the Cu nanocubes, in which the strongest diffraction peak is (200). This is different from the conventional power XRD pattern of fcc Cu (JCPDS #03-1018). It should be noted that the XRD sample was prepared by dropwise adding the Cu nanocube solution onto a glass slide followed by slow evaporation of toluene in a thermostat. As a result, almost all of the Cu nanocubes have a preferred orientation with {100} facets parallel to the substrate. Tilting experiments were carried out to determine the structure of Cu nanocubes. The diffraction patterns acquired from all of the examined particles can be assigned to the [001] zone axis without exception (Figure 3c), which reveals that the as-prepared Cu nanocubes are single crystals covered by six {100} facets. Figure 3d displays the SEM image of the Cu nanocubes with 2-4 layer stacking, where partially ordered structures in which Cu nanocubes are positioned in face-to-face configuration are observed.

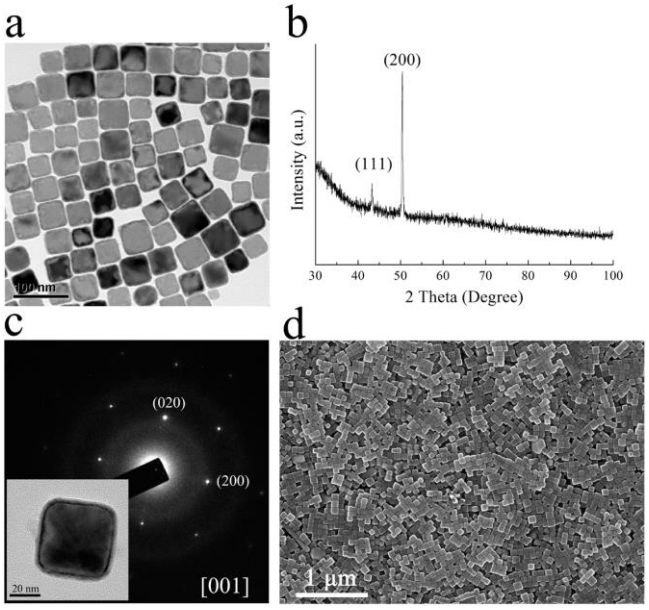

Figure 3. TEM image (a), XRD pattern (b), SAED pattern from a single Cu nanocube (insert) (c) and SEM image (d) of the Cu nanocubes with an average edge length of 46.8 nm.

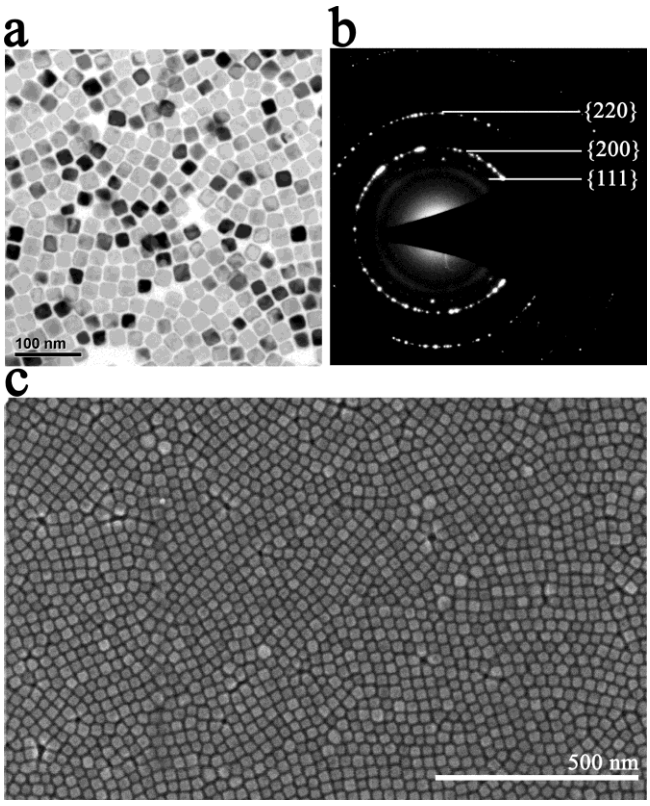

Figure 4. TEM image (a), SAED pattern (b) and SEM image (c) of the Cu nanocubes with an average edge length of 24.1 nm.

The amount of TOPO and the reaction temperature were found to play important roles in determining the final size of Cu nanocubes. For example, it was straightforward to increase the edge length of the Cu nanocubes to 76.4 nm (Figure S8a and S8b) simply by reducing the content of TOPO to 0.5 mmol in the typical synthetic procedure, although a small number of Cu nanowires were also present in the product (Figure S9). On the contrary, monodisperse Cu nanocubes with an average edge length of 24.1 nm were obtained (Figure 4a and S10) when the amount of TOPO was increased to 5 mmol and the reaction temperature was reduced to 210 ^{o}C. In the SAED pattern acquired from the area shown in Figure 4b, the diffraction ring owing to {111} facets almost disappears, while the diffraction ring owing to {200} facets becomes

stronger than all of the others, revealing the preferred orientation of the sample. Because these Cu nanocubes have a monodisperse size distribution and are well dispersed in toluene solution, they can be easily assembled onto silicon wafer (Figure 4c) by the method illustrated in Figure S5. Cu nanocubes with other different sizes are shown in Figure S11 and S12. The above results indicate that not only the shape but also the size of Cu nanocrystals is tunable by adjusting the reaction condition in this facile one-pot procedure.

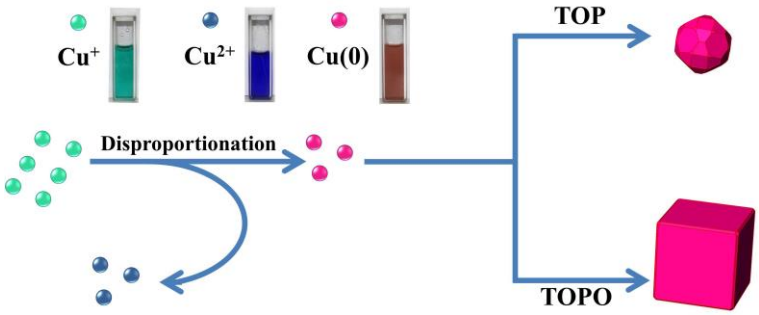

Scheme 1. Schematic illustration of the shape-selective formation of Cu nanospheres and nanocubes *via* the disproportionation reaction route.

Discussion of the Formation Mechanism. The formation mechanism of the as-prepared Cu nanocrystals was further investigated, and the overall process is illustrated in Scheme 1. CuBr, which is insoluble in water, was dissolved into organic solution by forming coordination complexes with oleylamine. The disproportionation reaction can be determined by the color change of the mixed solution. Green solution was formed by heating the mixture of oleylamine and CuBr at 80 ^{o}C, which can be attributed to the presence of Cu^{+}-oleylamine complexes. Figure 5 compares the FTIR spectra of oleylamine and Cu^{+}-oleylamine complexes. The stretching vibrations of N-H and C=C can be detected at about 3322.1 cm^{-1} and 1652.6 cm^{-1}, respectively (Figure 5, spectrum a), which are the characteristic peaks of oleylamine.[36] In the FTIR spectrum

of Cu^{+}-oleylamine (Figure 5, spectrum b), the N-H stretching region shifts to 3230.5 cm^{-1} and an obvious broadening in the band width is observed, which may be due to the coordination of Cu^{+} with amine group of oleylamine.[37] On the other hand, there was blue solution observed in the mother liquid after reaction, indicating a remnant of bivalent copper ions. For comparison, when $CuBr_2$ was used as precursor instead of CuBr, the particles produced had micron-scale size and chaotic shape after aging at 300 ^{o}C for 6 h. This is because a high temperature is necessary to reduce Cu^{2+} into Cu^{0} directly, but under such drastic reaction conditions the Cu crystals grow rapidly and chaotically, as mentioned previously. The disproportionation reaction enables the generation of zero valent Cu atoms at a relative low temperature so as to keep the growth of Cu nanocrystals under control of the capping agents.

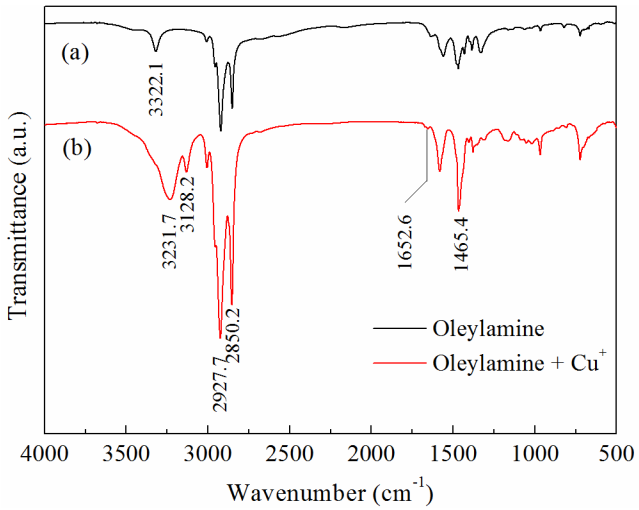

Figure 5. FTIR spectra of (a) oleylamine and (b) Cu^{+}-oleylamine complexes.

It was found that both TOP and TOPO could promote the disproportionation reaction, in other words, the reaction temperature was brought down by the addition of TOP or TOPO. Visible evidence of the reaction was obtained when the color of the mixed solution began to turn to red, which indicated the formation of Cu clusters at 190 ^{o}C and 240 ^{o}C in the presence of TOPO and

TOP, respectively. In contrast, this critical temperature increased to about 260 ^{o}C in the absence of either TOP or TOPO. The difference in the critical reaction temperature between TOP and TOPO also revealed the stronger coordination effect in the Cu^{+}-TOP complexes compared to Cu^{+}-TOPO complexes. The coordination interaction between metallic ions and ligands can be well explained by the HSAB (Hard-Soft-Acid-Base) theory. It is well known that Cu^{+} is a soft acid, while TOP (in the type of R_3P) is a soft base. However, in TOPO, oxygen (which is a well-known hard base) will act as the coordination atom instead of phosphorus. Therefore, it is reasonable to deduce that Cu^{+}-TOP is more stable than that of Cu^{+}-TOPO complexes. The shape-selective effect of TOP and TOPO (illustrated in Scheme 1) is based on their different coordination effects to Cu^{+}.[15] Firstly, the much stronger coordination of TOP to Cu^{+} prevents the metallic ions from being fast reduced to Cu(0), which seems to be necessary to accumulate enough reactant species to reach the critical nucleation concentration to achieve instantaneous nucleation at a higher temperature (260 ^{o}C).[38] The high reaction temperature avails the formation of isotropous crystals and weakens the selective adsorption of Br^{-}, which make the seeds grow equally in all directions into spherical-shaped crystals. Secondly, the synergistic effect of halogen anions and TOPO is necessary for the formation of a cuboidal geometry. Once TOP was replaced by TOPO, which possessed weaker coordination effect to Cu^{+}, the nucleation process would happen at a relatively lower temperature (170 ^{o}C). The lower reaction temperature enables a slow growth rate. The {100} facets of the Cu crystal seeds would be selectively capped by Br^{-} ions. From the Auger spectra acquired from the surface of Cu nanocubes, an obvious peak at 1398.5 eV belonging to the Br LMM transition (Figure 6a) is observed, indicating the binding of Br^{-} ions on Cu surfaces. However, in the Auger spectrum (Figure 6b) that covers P LMM region, no peak is observed. A similar phenomenon is also found from the Auger spectra acquired from

Cu nanospheres. This reveals that bromine ions have a stronger binding affinity than that of TOP or TOPO. The face-selective adsorption of halide anions has been well discussed in former reports.[20, 27] As a result, the other facets grew at a faster rate than the {100} facets. This kinetic difference led to the formation of Cu nanocubes instead of nanospheres.

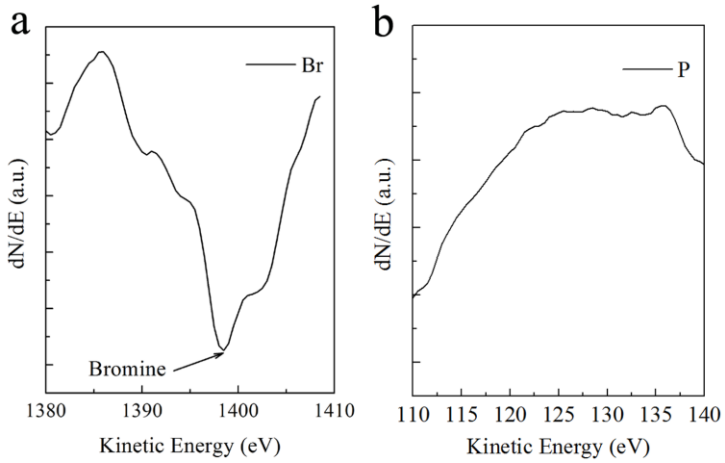

Figure 6. Auger spectra from the surface of Cu nanocubes. (a) Br LMM region; (b) P LMM region.

Optical Properties. By controlling the geometry of noble metal nanocrystals, such as Ag[11,39] and Au,[40-42] researchers have successfully tailored the optical responses of metallic nanocrystals and set the SPR at a specific wavelength for particular application. Here we study the shape-dependent optical characteristics of Cu nanocrystals. Among group IB metallic nanospheres, Cu displays the largest onset wavelength of interband transitions in the extinction spectrum[43] (about 600 nm, the green shadow area in Figure 7), which results in the weakest SPR intensity because of their location in the interband transition region. However, as can be seen in the extinction spectrum of the monodisperse Cu nanoparticles suspending in toluene solution (Figure 7a), there is still a strong and narrow SPR peak at 576 nm overlapping on the background absorption

induced by the interband transitions. Given the monodispersity of the as-synthesized Cu nanospheres, the coherent oscillation of the free conduction electrons could be excited by light within a very narrow wavelength region, which leads to the enhanced SPR absorption. According to Mie scattering theory, there should be a single SPR peak in the extinction spectrum of Cu nanospheres because of their spherically symmetric geometry,[43, 44] which is identical with our spectroscopic observation shown in Figure 7a.

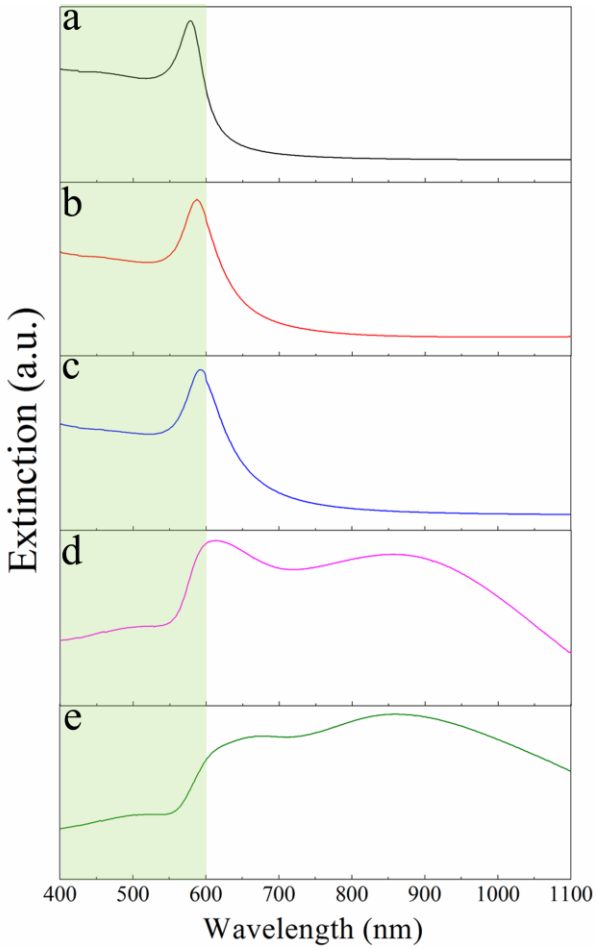

Figure 7. Vis-NIR extinction spectra of Cu nanospheres with an average diameter of 23.4 nm (a) and nanocubes with an average edge length of 24.1 nm (b), 26.4 nm (c), 30.7 nm (d) and 46.8 nm (e), respectively. All of the spectra are acquired from the Cu nanocrystals suspended in toluene.

In respect to the extinction spectra of Cu nanocubes (Figure 7b to 7e), there is a tiny red shift from 576 to 585 nm as the edge length of the nanocubes increases from 24.1 to 26.4 nm (see Figure S11 for TEM image). Interestingly, when the edge length of Cu nanocubes reaches 30.7 nm (see Figure S12 for TEM image), two new SPR peaks appear at about 610 nm and about 855 nm. In the case of even larger cubes, such as the 46.8 nm cubes, these two new peaks are at about 670 and 858 nm. According to former reports,[17] the red-shift may be due to the larger dimension of Cu nanocubes compared with Cu nanospheres. Similar phenomena have been observed in gold nanoparticles with well-controlled sizes.[45, 46] Furthermore, the double-peaked feature in the spectrum of the 30.7 and 46.8 nm cubes is evidently caused by their aggregation into more complex structures. From the TEM images (Figure 4 and S11), it can be seen that Cu nanocubes with a smaller sizes (24.1 nm and 26.4 nm) do not contact by each other due to the separation of capping agents. However, the van der Waals attractions between Cu nanocubes with larger sizes will be relatively stronger, and in this case the capping molecules may exert insufficient repulsion. As a result, the formation of aggregates (see Figure S13) such as dimers and trimers may lead to SPR peaks at longer wavelengths.

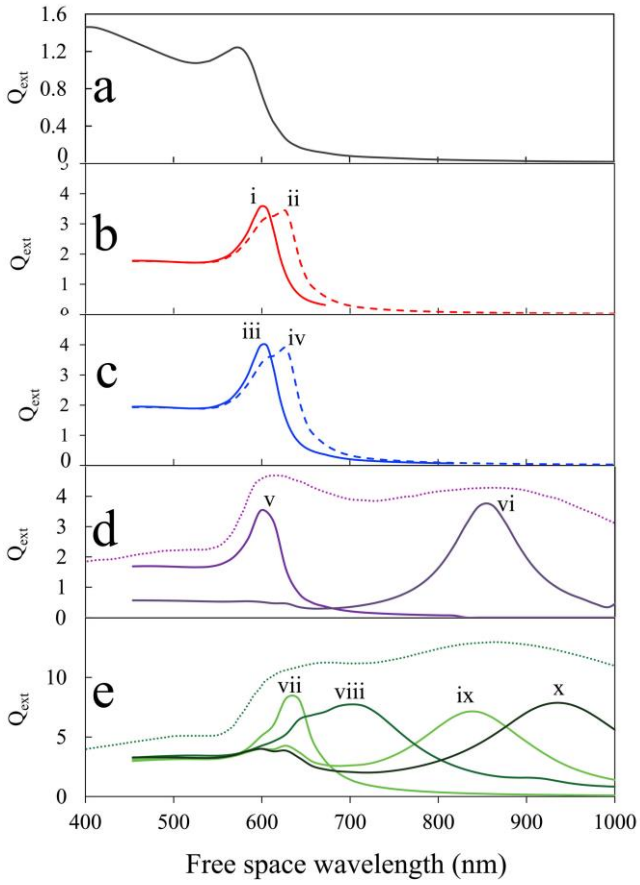

Figure 8. Calculated extinction efficiencies of colloidal suspensions of Cu nanospheres and nanocubes in toluene, (a) isolated 23.4 nm diameter nanospheres, (b) isolated 24.1 nm nanocubes, *i*= rounded edges, *ii*= sharp edges, (c) isolated 26.1 nm nanocubes, *iii*= rounded edges, *iv*= sharp edges, (d) mixture of isolated 30.7 nm cubes and their linear trimers, *v*=single cubes, *vi*=three cubes in a row (experimental data is shown for comparison as a dotted line) (e) calculated extinction spectra of 46.8 nm cubes in various configurations, *vii*=single cubes, *viii*=four cubes in a 2x2 arrangement, *ix*=three cubes in a row, *x*=four cubes in row. (experimental data is shown for comparison as a dotted line).

To better understand the optical properties of the as-prepared Cu nanocrystals, we performed theoretical simulations of their extinction spectra, for single cubes, linear chains of up to five cubes, L-shaped aggregates of three cubes, and four cubes in a square arrangement (Figure 8). These shapes were chosen because they had been observed in TEM samples of these cubes. The transverse plasmon resonance peaks of the simulation of the single cubes, Figure 6a, are a reasonable match to the higher energy peaks of the experimental data with any residual small discrepancies between the two probably due to a lack of geometric perfection in the experimental nanoparticles. The simulated peaks for single cubes of maximum theoretical edge sharpness are somewhat triangular in shape because the simulation has generated some higher order resonances of the transverse resonance peak. This phenomenon has been observed before in Ag cuboids.[9] Therefore, it was necessary to generate single cubes with slightly rounded edges to better match the experimental data.

As mentioned, experimental samples with cube sizes of 30.7 and 46.8 nm also showed a second broad resonance centered on about 860 nm. The simulations suggest that even two cubes in a side-by-side cannot generate such a deeply red-shifted resonance, and it appears necessary to invoke the existence of aggregates containing at least three, four and five cubes to explain them. Spectra very similar in nature to the measured ones could be obtained by producing an ensemble average of such aggregated cubes, with the broader peaks of the experimental data being probably due to the presence of a small spread in cube dimensions. A breakdown of the shapes necessary to match the experimental spectrum is shown in Figure 8e for the case of the 46.8 nm cubes. A similar breakdown (not shown) applied in the case of the 30.7 nm cubes. In these simulations an inter-particle gap about 1.9 nm is necessary in order to provide the correct peak positions.

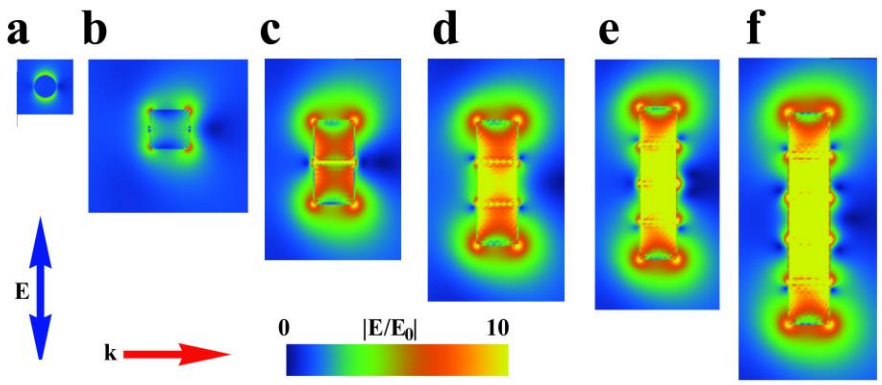

Figure 9. Calculated electric field intensities (shown as the norm, ||E||) at the plasmon resonance frequencies of selected Cu nanocrystals or nanocrystal aggregates in toluene. Crystals and fields are shown at the same scales. (a) 23.4 nm diameter sphere irradiated at 573 nm, (b) single 46.8 nm cube (edges have been rounded) irradiated at 613 nm, (c) longitudinal plasmon resonance of two 46.8 nm cubes in a line irradiated at 647 nm (d) longitudinal plasmon resonance of three 46.8 nm cubes in a line irradiated at 709 nm, (e) longitudinal plasmon resonance of four 46.8 nm cubes in a line irradiated at 934 nm, (f) longitudinal plasmon resonance of five 46.8 nm cubes in a line irradiated at 1022 nm. (A separation gap of 1.9 nm was used for the muti-cube geometries.)

The numerical simulations show that the electric field intensity on the individual Cu nanospheres is relatively low compared to that of the nanocubes, Figure 9. The cubes are not only better nano-antennas for geometric reasons but, importantly, their characteristic resonance frequencies are also well away from the damping effect of copper's interband transitions in the mid to lower-wavelengths of visible light. Given that aggregation of the larger cubes occurred, it was interesting to also explore the electric field intensities of the assembled structures of two, three, four and five cubes. The increase in overall electric field intensity as the longitudinal

resonance of the aggregates is red-shifted is quite apparent in Figure 9. Notice also that the fields at the sharp edges and in the gaps of these structures are very high relative to those of an isolated sphere or cube. Therefore, the aggregated structures may be more useful for some applications, such as SERS, than un-aggregated particles.

CONCLUSION

In summary, we have demonstrated a facile one-pot method that is based on a disproportionation reaction in oleylamine solvent. This technique provides a shape-selective synthesis of Cu nanocrystals with spherical and cubic morphology as well as with very narrow size distribution. Owing to the relative mild reaction conditions and capping agents, the growth of Cu nanocrystals was kept under kinetic control. Monodispersed Cu nanospheres were generated when TOP was introduced as a capping agent, while TOPO could be used for the synthesis of monodisperse Cu nanocubes with tunable sizes. Furthermore, the optical properties of the as-prepared Cu nanocrystals were investigated both experimentally and theoretically. A strong and narrow SPR peak at 576 nm was observed for the Cu nanospheres, while the SPR peaks of Cu nanocubes exhibited a red-shift that increased with their sizes. Theoretical simulations on the extinction spectra agree well with the observed spectra. While the smaller cubes evidently stayed dispersed as single entities, the optical properties of suspensions of the cubes with larger sizes (30.7 nm and 46.8 nm) suggested that they had aggregated into triple, quadruple or even pentuple structures. The reported simple strategy for the synthesis of Cu nanocrystal in this study not only provides a convenient access to the further investigation of their physical properties due to their shape and reasonable size singularity but also may promote the application of Cu nanocrystals in photonic and nanoelectronic devices due to their comparatively lower cost than Au or Ag.

AUTHOR INFORMATION

Corresponding Authors

*Email: yuanzhi@xmu.edu.cn; dlpeng@xmu.edu.cn

ACKNOWLEDGMENT

The authors gratefully acknowledge the financial support from the National Basic Research Program of China (No. 2012CB933103), the National Outstanding Youth Science Foundation of China (Grant No. 50825101), the National Natural Science Foundation of China (Grant Nos. 51171157 and 51371154), the program of China Scholarships Council (No. 201206315023), the Australian Research Council and the UTS High Performance Computing Cluster.

ASSOCIATED CONTENT

Supporting Information. Synthetic details, TEM and HRTEM images, size distribution histograms and self-assembly scheme. This material is available free of charge via the Internet at http://pubs.acs.org.

REFERENCES

(1) Kao, C.-S.; Chen, F.-C.; Liao, C.-W.; Huang, M. H.; Hsu, C.-S. Plasmonic-Enhanced Performance for Polymer Solar Cells Prepared with Inverted Structures. *Appl. Phys. Lett.* **2012**, *101*, 193902–193904.

(2) Wu, J.-L.; Chen, F.-C.; Hsiao, Y.-S.; Chien, F.-C.; Chen, P.; Kuo, C.-H.; Huang, M. H.; Hsu, C.-S. Surface Plasmonic Effects of Metallic Nanoparticles on the Performance of Polymer Bulk Heterojunction Solar Cells. *ACS Nano* **2011**, *5*, 959–967.

(3) Shao, M.-W.; Lu, L.; Wang, H.; Wang, S.; Zhang, M.-L.; Ma, D.-D.-D.; Lee, S.-T. An Ultrasensitive Method: Surface-Enhanced Raman Scattering of Ag Nanoparticles from β-Silver Vanadate and Copper. *Chem. Commun.* **2008**, 2310–2312.

(4) Wang, H.; Levin, C. S.; Halas, N. J. Nanosphere Arrays with Controlled Sub-10-nm Gaps as Surface-Enhanced Raman Spectroscopy Substrates. *J. Am. Chem. Soc.* **2005**, *127*, 14992–14993.

(5) Larsson, E. M.; Alegret, J.; Käll, M.; Sutherland, D. S. Sensing Characteristics of NIR Localized Surface Plasmon Resonances in Gold Nanorings for Application as Ultrasensitive Biosensors. *Nano Lett.* **2007**, *7*, 1256–1263.

(6) Huang, Y.; Wu, L.; Chen, X.; Bai, P.; Kim, D.-H. Synthesis of Anisotropic Concave Gold Nanocuboids with Distinctive Plasmonic Properties. *Chem. Mater.* **2013**, *25*, 2470–2475.

(7) Xia, Y.; Xiong, Y. J.; Lim, B.; Skrabalak, S. E. Shape-Controlled Synthesis of Metal Nanocrystals: Simple Chemistry Meets Complex Physics? *Angew. Chem. Int. Ed.* **2009**, *48*, 60–103.

(8) Pelton, M.; Aizpurua, J.; Bryant, G. Metal-Nanoparticle Plasmonics. *Laser Photonics Rev.* **2008**, *2*, 136–159.

(9) Cortie, M. B.; Liu, F.; Arnold, M. D.; Niidome, Y. Multimode Resonances in Silver Nano-Cuboids. *Langmuir* **2012**, *28*, 9103–9112.

(10) Huang, M. H.; Lin, P.-H. Shape-Controlled Synthesis of Polyhedral Nanocrystals and Their Facet-Dependent Properties. *Adv. Funct. Mater.* **2012**, *22*, 14–24.

(11) Jin, R.; Cao, Y.; Mirkin, C. A.; Kelly, K. L.; Schatz, G. C.; Zheng, J. G. Photoinduced Conversion of Silver Nanospheres to Nanoprisms. *Science* **2001**, *94*, 1901–1903.

(12) Pedersen, D. B.; Wang, S. Surface Plasmon Resonance Spectra of 2.8 ±0.5 nm Diameter Copper Nanoparticles in Both Near and Far Fields. *J. Phys. Chem. C* **2007**, *111*, 17493–17499.

(13) Salzemann, C.; Lisiecki, I.; Urban, J.; Pileni, M. P. Anisotropic Copper Nanocrystals Synthesized in a Supersaturated Medium: Nanocrystal Growth. *Langmuir* **2004**, *20*, 11772–11777.

(14) Salzemann, C.; Brioude, A.; Pileni, M. P. Tuning of Copper Nanocrystals Optical Properties with Their Shapes. *J. Phys. Chem. B* **2006**, *110*, 7208–7212.

(15) Mott, D.; Galkowski, J.; Wang, L.; Luo, J.; Zhong, C.-J. Synthesis of Size-Controlled and Shaped Copper Nanoparticles. *Langmuir* **2007**, *23*, 5740–5745.

(16) Pastoriza-Santos, I.; Sánchez-Iglesias, A.; Rodríguez-González, B.; Liz-Marzán, L. M. Aerobic Synthesis of Cu Nanoplates with Intense Plasmon Resonances. *small* **2009**, *5*, 440–443.

(17) Jin, M.; He, G.; Zhang, H.; Zeng, J.; Xie, Z.; Xia. Y. Shape-Controlled Synthesis of Copper Nanocrystals in an Aqueous Solution with Glucose as a Reducing Agent and Hexadecylamine as a Capping Agent. *Angew. Chem. Int. Ed.* **2011**, *50*, 10560–10564.

(18) Ye, E.; Zhang, S.-Y.; Liu, S.; Han, M.-Y. Disproportionation for Growing Copper Nanowires and Their Controlled Self-Assembly Facilitated by Ligand Exchange. *Chem. Eur. J.* **2011**, *17*, 3074–3077.

(19) Huang, X.; Chen, Y.; Chiu, C.-Y.; Zhang, H.; Xu, Y.; Duan, X.; Huang, Y. A Versatile Strategy to the Selective Synthesis of Cu Nanocrystals and the in situ Conversion to CuRu Nanotubes. *Nanoscale* **2013**, *5*, 6284–6290.

(20) Guo, H.; Chen, Y.; Ping, H.; Jin, J.; Peng, D.-L. Facile Synthesis of Cu and Cu@Cu-Ni Nanocubes and Nanowires in Hydrophobic Solution in the Presence of Nickel and Chloride Ions. *Nanoscale* **2013**, *5*, 2394–2402.

(21) Jeong, S.; Woo, K.; Kim, D.; Lim, S.; Kim, J. S.; Shin, H.; Xia, Y.; Moon, J. Controlling the Thickness of the Surface Oxide Layer on Cu Nanoparticles for the Fabrication of Conductive Structures by Ink-Jet Printing. *Adv. Funct. Mater.* **2008**, *18*, 679–686.

(22) Pootawang, P.; Saito, N.; Lee, S. Y. Discharge Time Dependence of a Solution Plasma Process for Colloidal Copper Nanoparticle Synthesis and Particle Characteristics. *Nanotechnology* **2013**, *24*, 055604.

(23) Wang, F.; Richards, V. N.; Shields, S. P.; Buhro, W. E. Kinetics and Mechanisms of Aggregative Nanocrystal Growth. *Chem. Mater.* **2014**, *26*, 5–21.

(24) Liao, H.-G.; Cui, L.; Whitelam, S.; Zheng, H. Real-Time Imaging of Pt_3Fe Nanorod Growth in Solution. *Science* **2012**, *336*, 1011–1014.

(25) Xie, S.; Peng, H.-C.; Lu, N.; Wang, J.; Kim, M. J.; Xie, Z.; Xia, Y. Confining the Nucleation and Overgrowth of Rh to the {111} Facets of Pd Nanocrystal Seeds: The Roles of Capping Agent and Surface Diffusion. *J. Am. Chem. Soc.* **2013**, *135*, 16658–16667.

(26) Chen, M.; Wu, B.; Yang, J.; Zheng, N. Small Adsorbate-Assisted Shape Control of Pd and Pt Nanocrystals. *Adv. Mater.* **2012**, *24*, 862–879.

(27) DuChene, J. S.; Niu, W.; Abendroth, J. M.; Sun, Q.; Zhao, W.; Huo, F.; Wei, W. D. Halide Anions as Shape-Directing Agents for Obtaining High-Quality Anisotropic Gold Nanostructures. *Chem. Mater.* **2013**, *25*, 1392–1399.

(28) Lohse, S. E.; Burrows, N. D.; Scarabelli, L.; Liz-Marzán, L. M.; Murphy, C. J. Anisotropic Noble Metal Nanocrystal Growth: The Role of Halides. *Chem. Mater.* **2014***, 26,* 34–43.

(29) Peng, S.; Sun, Y. Synthesis of Silver Nanocubes in a Hydrophobic Binary Organic Solvent. *Chem. Mater.* **2010**, *22*, 6272–6279.

(30) Yang, H.-J.; He, S.-Y.; Chen, H.-L.; Tuan, H.-Y. Monodisperse Copper Nanocubes: Synthesis, Self-Assembly, and Large-Area Dense-Packed Films, *Chem. Mater.* **2014**, *26*, 1785–1793.

(31) Guo, H.; Chen, Y.; Ping, H.; Wang, L.; Peng, D.-L. One-Pot Synthesis of Hexagonal and Triangular Nickel-Copper Alloy Nanoplates and Their Magnetic and Catalytic Properties. *J. Mater. Chem.* **2012**, *22*, 8336–8344.

(32) Draine, B.T.; Flatau, P. J. The Discrete Dipole Approximation for Periodic Targets: I. Theory and Test. *J. Opt. Soc. Am. A* **2008**, *25*, 2693–2703.

(33) Weaver, J. H.; Frederikse, H. P. R. Optical Properties of Selected Elements, in CRC Handbook of Chemistry and Physics. 82 ed. (Ed: D. R. Lide), CRC Press, Boca Raton, 2001.

(34) Kedenburg, S.; Vieweg, M.; Gissibl, T.; Giessen, H. Linear Refractive Index and Absorption Measurements of Nonlinear Optical Liquids in the Visible and Near-Infrared Spectral Region. *Opt. Mater. Express* **2012**, *2*, 1588–1611.

(35) Debenham, M.; Dew, G. D. The Refractive Index of Toluene in the Visible Spectral Region. *J. Phys. E: Sci. Instrum.* **1981**, *14*, 544–545.

(36) Luo, J.; Han, L.; Kariuki, N. N.; Wang, L.; Mott, D.; Zhong, C.-J.; He, T. Synthesis and Characterization of Monolayer-Capped PtVFe Nanoparticles with Controllable Sizes and Composition. *Chem. Mater.* **2005**, *17*, 5282–5290.

(37) Cooper, J. K.; Franco, A. M.; Gul, S.; Corrado, C.; Zhang, J. Z. Characterization of Primary Amine Capped CdSe, ZnSe, and ZnS Quantum Dots by FT-IR: Determination of Surface Bonding Interaction and Identification of Selective Desorption. *Langmuir*, **2011**, *27*, 8486–8493.

(38) Tao, A. R.; Habas, S.; Yang, P. Shape Control of Colloidal Metal Nanocrystals. *small*, **2008**, *4*,310–325.

(39) Guo, H.; Chen, Y.; Chen, X.; Wen, R.; Yue, G.-H.; Peng, D.-L. Facile Synthesis of Near-Monodisperse Ag@Ni Core-Shell Nanoparticles and Their Application for Catalytic Generation of Hydrogen. *Nanotechnology* **2011**, *22*, 195604.

(40) Kim, D. Y.; Yu, T.; Cho, E. C.; Ma, Y.; Park, O. O.; Xia, Y. Synthesis of Gold Nano-hexapods with Controllable Arm Lengths and Their Tunable Optical Properties. *Angew. Chem. Int. Ed.* **2011**, *50*, 6328–6331.

(41) Nehl, C. L.; Liao, H.; Hafner, J. H. Optical Properties of Star-Shaped Gold Nanoparticles. *Nano Lett.* **2006**, *6*, 683–688.

(42) Aizpurua, J.; Hanarp, P.; Sutherland, D. S.; Käll, M.; Bryant, G. W.; García de Abajo F. J. Optical Properties of Gold Nanorings. *Phys. Rev. Lett.* **2003**, *90*, 057401.

(43) Wang, H.; Tam, F.; Grady, N. K.; Halas, N. J. Cu Nanoshells: Effects of Interband Transitions on the Nanoparticle Plasmon Resonance. *J. Phys. Chem. B* **2005**, *109*, 18218–18222.

(44) Zhang, L.; Jing, H.; Boisvert, G.; He, J. Z.; Wang, H. Geometry Control and Optical Tunability of Metal–Cuprous Oxide Core–Shell Nanoparticles. *ACS Nano* **2012**, *6*, 3514–3527.

(45) Li, C.; Shuford, K. L.; Chen, M.; Lee, E. J.; Cho, S. O. Facile Polyol Route to Uniform Gold Octahedra with Tailorable Size and Their Optical Properties. *ACS Nano* **2008**, *2*, 1760–1769.

(46) Kim, D. Y.; Li, W.; Ma, Y.; Yu, T.; Li, Z.-Y.; Park, O. O.; Xia, Y. Seed-Mediated Synthesis of Gold Octahedra in High Purity and with Well-Controlled Sizes and Optical Properties. *Chem. Eur. J.* **2011**,*17*, 4759–4764.

TOC GRAPHICS